JOURNAL OF MATERIALS SCIENCE 25 (1990) 4792–4803

Slip patterns in sliding sphere experiments on (1 1 1) single crystal MnZn ferrite

A. BROESE VAN GROENOU, S. E. KADIJK
Philips Research Laboratories, P.O. Box 80000, 5600 JA Eindhoven, The Netherlands

By sliding a 0.25 mm radius ruby sphere on a (1 1 1) MnZn ferrite crystal, grooves have been made at speeds from 4 to 400 μm sec^{-1}, at loads from 0.5 to 4 N and after 1 to 1000 passes. The deformation is observed by microscopy and profilometry. For a single pass slip lines are observed in all directions of sliding, above a load that increases with sliding speed. Slip-line patterns are identified as due to $\{1\,0\,0\}\langle 0\,1\,1\rangle$ slip, coupled to $\{1\,1\,1\}\langle 0\,1\,1\rangle$ slip, as in earlier work on pencil patterns in indentations. At higher speeds of sliding the number of $\{1\,0\,0\}$ lines decreases due to lack of nucleation of dislocations. The cross-slip to $\{1\,1\,1\}$, in general, shows an even stronger speed dependence. The number of slip lines at a given load and speed depends on the direction of sliding. Along $\langle 0\,1\,1\rangle$ the density is largest. Along $\langle \bar{2}\,1\,1\rangle$ the density and the groove depth change when the direction is reversed. The angular variation is not determined by the (small) variations of the resolved shear stress, but by the necessity of repeated nucleation of slip. Curved slip lines are observed in several directions of sliding. The curvature is attributed to multiple cross-slip, from $\{1\,1\,1\}$ back to $\{1\,0\,0\}$. Powder-like debris is formed during sliding by fracture of the slip steps. The powder is then transported to the sides of the groove by repeated sliding.

1. Introduction

1.1. Anisotropy

Manganese zinc ferrites with the cubic spinel structure are magnetic materials that have found many applications in inductors and transformers. Single crystals are used in heads for magnetic recording, where the mechanical properties are also important. The resistance to wear by recording tapes is high on the (1 0 0) plane, but much lower on (1 1 1). Hirota and colleagues [1, 2] give a wear rate of 23 μm h^{-1} on (1 1 1) along $\langle 0\,\bar{1}\,1\rangle$ and 8 μm h^{-1} on (1 1 1) along $\langle \bar{2}\,1\,1\rangle$, but only 0.5 μm h^{-1} on (1 0 0) along $\langle 0\,\bar{1}\,1\rangle$. If plastic deformation gives the main contribution to the wear process in a recorder, the stress–strain curve should also show considerable anistropy. However, if the yield stress is derived from the Knoop [3] or Vickers hardness [4, 5], that vary from 5.9 to 6.8 GPa, the variation is not more than $\pm 5\%$.

There are, however, other measures of plastic deformation that do show anisotropy, e.g. the depth of indentations or grooves made by a loaded sphere and the corresponding slip line patterns. For sliding, Stein's work on TiO_2 is an example [6], and for rolling, that on MgO by Dufrane and Glaeser [7], both at room temperature. Indentations on MnZn ferrite crystals by the present authors showed simple slip patterns at low loads and short times, which became more complicated at high loads, longer times or, in the case of grooves, after more passes [8–12]. Here too, there is a dependence on the crystal plane that is loaded. The variation between the various planes is illustrated by the stress where slip first appears. In terms of P_0, the maximum stress in the contact, slip appeared on (1 0 0) at a stress of 6.5 GPa, on (1 1 1) at 4.9 GPa and on (1 1 0) at 7.0 GPa. These values hold after indentation for 3 sec; for longer times the values are lower. The larger wear on (1 1 1), combined with the low stress needed for deformation, led us to investigate in more detail the deformation processes on this plane.

1.2. Grooves

The anisotropy of plastic deformation shows up clearly in grooves made by a sliding sphere. The groove depth (d) is a function of load (F_n), speed (v) and number of passes (N). The following relation is approximately valid at room temperature [12]

$$d = C_1 F_n + C_2 \log_{10} N + C_3 \log_{10} v + C_4 \quad (1)$$

over the range 0.4 to 400 μm sec^{-1} for v and 1 to 1000 for N. For example, for sliding on (1 1 1) along $\langle 0\,1\,\bar{1}\rangle$

$$d = 85(\pm 9) F_n + 90(\pm 12) \log_{10} N - 49(\pm 15) \log_{10} v - 81(\pm 46) \quad (2)$$

where F_n is in Newtons and v in μm sec^{-1}. The numbers between brackets give the sample standard deviation. For sliding on (1 1 1) along $\langle \bar{2}\,1\,1\rangle$, the depth is given by

$$d = 73(\pm 5) F_n + 55(\pm 7) \log_{10} N - 27(\pm 8) \log_{10} v - 29(\pm 24). \quad (3)$$

The last coefficient, C_4, is negative, whereas C_1 is positive. This combination describes the threshold in load necessary for a groove to be observed. The threshold depends on the conditions of sliding. For

0022–2461/90 $03.00 + .12

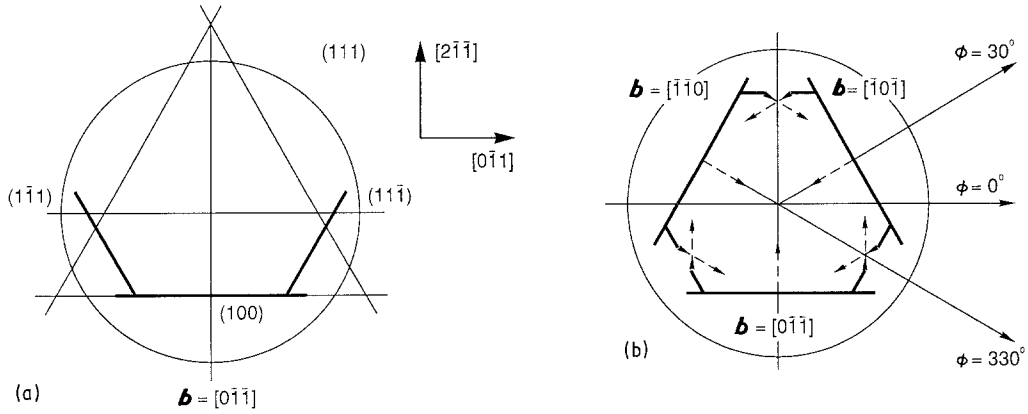

Figure 1 Schematic patterns of slip on (1 1 1). (a) Pattern for one Burger's vector, [0 $\bar{1}$ $\bar{1}$], showing the (1 0 0) slip on the basis of the triangle, and two {1 1 1} lines that start at the base. The position of the contact circle is indicated, as well as the orientation of the cubic axes of the sample. (b) Pattern for three Burger's vectors, showing all sides of the triangle, due to {1 0 0} slip, and the cross-over lines on {1 1 1} that start on the sides. The short arrows indicate the projection of the position of the maximum RSS, from where slip proceeds to the surface. The directions of sliding are indicated by the angle ϕ.

$N = 1$ and $v = 1\,\mu m\,sec^{-1}$ it varies from 0.4 N for sliding along $\langle\bar{2}\,1\,1\rangle$ on (1 1 1), to 1.0 N along $\langle 0\,1\,\bar{1}\rangle$ on the same plane, and to 2.3 N on (0 0 1) along $\langle 1\,1\,0\rangle$.

1.3. Slip after indenting (1 1 1)

Indentations on several planes of ferrite resulted in remarkably clear slip line patterns on the surface. These could be identified to be due to slip on several systems, all with $\langle 1\,1\,0\rangle$ Burgers vectors [8]. For (1 1 1) the pattern is shown schematically in Fig. 1a at a low load where only one specific Burgers vector, [0 $\bar{1}$ $\bar{1}$], is active. There is a long baseline due to slip on the (1 0 0) plane, with two short lines at the ends, where slip has crossed on to (1 1 $\bar{1}$) and (1 $\bar{1}$ 1). The orientation of the crystal axes is important to identify the triangle as due to {1 0 0} and not {1 1 1} (Fig. 1a). If all $\{1\,0\,0\}\langle 0\,1\,1\rangle$ systems are activated, a triangular pattern of slip lines is observed (Fig. 1b). The cross-slip lines on {1 1 1} are parts of an inverse triangle. In all cases there were only small traces of lines due to the $\{1\,1\,0\}\langle 1\,1\,0\rangle$ system.

1.4. Resolved shear stress

Calculations of the resolved shear stress (RSS) have contributed to the identification of the line patterns [9, 10]. The RSS on a slip plane was calculated by Schmidt's formula using the stress distribution underneath a loaded sphere, as given by Hamilton and colleague [13, 14]. The elastic modulus and the Poisson constant of $Mn_{0.62}Zn_{0.32}Fe_{2.06}O_4$ were taken from de With and Damen [15]. The radius of the contact circle, a, and the maximum stress in the contact, P_0, are derived from the Hertz equations [17]. In this elastic approximation the values of RSS/P_0 for a number of slip systems have been calculated (Table I). The slip systems with a high value of RSS/P_0 need a low P_0 value to be activated and are therefore observed at lower loads. The position of the lines with respect to the contact circle has been calculated and agrees with the pattern found in indentations on (1 1 1) [10].

The $\{1\,0\,0\}\langle 0\,1\,1\rangle$ system, activated by indenting (1 1 1), is found at a lower RSS, 1.5 GPa, than $\{1\,1\,1\}\langle 0\,1\,1\rangle$ after indenting (0 0 1), 1.7 GPa. Indentations on (1 1 0) again show $\{1\,0\,0\}\langle 0\,1\,1\rangle$ slip to occur first, but at a higher RSS. (A possible reason is that the elastic tensor has been simplified in calculating the RSS [9, 10].)

1.5. Patterns in the grooves

Typically, for a groove pattern, slip lines along the direction of sliding are long, whereas lines at an angle to the groove end near the edge. These systems start from new nuclei, further along the groove, when activated by the stress field of the moving sphere. An example was found in sliding on (1 1 0) at 400 $\mu m\,sec^{-1}$ [11]. The {1 1 1} and {1 0 0} slip planes act independently, because for most directions of sliding on (1 1 0) the lines run out of the groove and reappear after renucleation. Under these conditions the stress at the maximum RSS may be combined with the strain deduced from the groove depth, into stress–strain curves for slip on {1 1 1} and {1 0 0} [11]. To calculate the RSS in the case of sliding, the tangential load due to friction must be included [13, 14].

1.6. Cross-slip

In general, however, cross-slip is present and plays a

TABLE I Primary and secondary slip systems with $\langle 1\,1\,0\rangle$ Burgers vectors in MnZn ferrite

Plane of indentation	Primary system			Secondary system		
	Plane	RSS/P_0	RSS (GPa)	Plane	RSS/P_0	RSS (GPa)
(1 0 0)	{1 1 1}	0.264	1.7	{1 0 0}	0.161	1.05
(1 1 1)	{1 0 0}	0.308	1.5	{1 1 1}	0.247	1.7
$(1\,1\,0)_{60}$	{1 0 0}	0.256	1.8	{1 1 1}	0.282	2.0
$(1\,1\,0)_0$	{1 0 0}	0.213	1.7	{1 1 1}	0.213	1.7

RSS/P_0 is calculated, P_0 is taken from [9, 10] to calculate RSS.

role in the anisotropic deformation of the material. When in indentations the number of slip lines is small, the RSS for cross-over can be calculated [10]. A clear difference between {1 1 1} and {1 0 0} is found. Once slip has started on {1 1 1}, cross-over to {1 0 0} occurs at RSS = 1.05 GPa, whereas for crossing from {1 0 0} to {1 1 1} a higher value, 1.7 GPa, is needed (Table I). This points again to the relative ease with which {1 0 0} can be activated in comparison to {1 1 1}. The values for the secondary systems are given in Table I.

1.7. Speed effects

The log v and log N terms in Equations 1 to 3 show that the groove depth depends on time and repetition. This holds for the slip patterns too. A complication is that the patterns in the groove show secondary slip as in the indentations [10, 11]. In sliding on (1 1 0), secondary slip with a vertical [1 1 0] Burgers vector is present at higher loads. Cross-over is observed between {1 0 0} and {1 1 1}, and {1 1 1} and {1 1 0} [11]. There is, however, a strong effect of sliding speed, because the patterns need more time to appear in the sequence {1 0 0}, {1 1 1} and {1 1 0}. One of the objects of the present work was to investigate whether the speed dependence also occurs during sliding on (1 1 1).

1.8. Nucleation and propagation

In sliding on (1 1 0) the influence of speed on groove depth, given by the coefficient C_3 in Equation 1, does not change with temperature [12]. If thermal activation does not limit the appearance of slip lines, what does? Is it propagation by another mechanism or nucleation? In the first case, a repeat of the sliding would give longer lines as well as more lines. If nucleation prevents the appearance of slip, a repeat, or lower speeds, would give more lines. The second object of this work was to address these questions by sliding on (1 1 1). The trigonal symmetry of the indentation patterns [11] makes an investigation of the angular variation of depth and patterns especially interesting. The direction of sliding will be given by the angle ϕ, defined in Fig. 1b. In this figure there are three directions of sliding that give symmetrical patterns, at $\phi = 0°$, 30° and 330°. Between 330° (= −30°) and 30° all independent sliding directions are available. Because of the equivalence of 330° and 210°, $\phi = 330°$ corresponds to the reversed motion of $\phi = 30°$.

1.9. The present work

In the experiments to be described, a small number of passes was used in order to study relatively simple line patterns as a function of speed and the number of passes. Low loads were used to avoid cracking. A number of general results will be given in Section 3, followed by details about the angular dependence (Section 4) and the speed dependence (Section 5). Special features of the patterns are discussed in Section 6.

2. Experimental procedure

Grooves were made by sliding a ruby sphere (diameter 0.50 mm) over a polished surface. The sliding apparatus consists of a balance, with a damping system on one arm, on the other arm an indentor, in this case a sphere. An x–y table carries the sample, which can be transported by a motor [8, 17].

Crystals of manganese zinc ferrite, $Mn_{0.62}Zn_{0.32}Fe_{2.06}O_4$, were used, made by the Bridgman technique. Blocks were cut and the surface of the (1 1 1) face was diamond polished. The centre line average roughness is 2 nm.

The grooves on the sample were observed after the experiment under a microscope equipped with Nomarski interference contrast. In most photographs to be shown the light comes from the north-west. The dimensions of the grooves were measured by means of a mechanical profiler, scanning perpendicular to the sliding direction. Grooves with a depth of 10 to 500 nm could be measured in this way.

3. Results

3.1. Single pass along [0 $\bar{1}$ 1], $\phi = 0°$

An example of a groove, made under a load of 4 N and at $v = 400\,\mu m\,sec^{-1}$, is shown in Fig. 2a. The triangle at the start is due to the indentation that is made before the motor starts. The sides of the triangle are due to primary slip on {1 0 0}. A schematic figure for the basic pattern is shown in Fig. 2b. Short lines due to slip on {1 1 1} are frequently found to be connected to the {1 0 0} base, indicating that slip crosses from {1 0 0} to {1 1 1} (Fig. 1a). When all sides of the triangle are excited, six lines are possible (Fig. 1b).

Returning now to the single-pass groove made at $\phi = 0°$ in Fig. 2a, one observes that the base of the triangle is not parallel to the groove. The white, (0 1 0), side of the triangle, formed at the leading side, is absent in the groove. The black trailing side, due to (0 0 1), recurs whenever the inclined base is replaced by a new one.

White lines, connected to the base line because of cross-slip to (1 1 $\bar{1}$)[0 $\bar{1}$ $\bar{1}$] (Fig. 2b), are abundantly present, with a neat periodicity of 5 to 6 μm. With about the same period the profile along the groove shows slip steps of 30 to 50 nm (Fig. 2c). The white lines end at about the centre of the triangle. Owing to the inclination of the base line, the cross-over lines become shorter until the comb ends after about 18 "teeth".

3.2. Single pass along ⟨2 1 1⟩, $\phi = 30°$ and 330°

When the direction of sliding is rotated to $\phi = 30°$, the pattern at 4 N and 400 $\mu m\,sec^{-1}$ consists of lines on the edges, leaving an empty space in the centre (Fig. 3a). There are lines pointing outwards due to slip on the (0 0 1) and (1 0 0) sides of the original triangle (Fig. 3b). These lines are spaced irregularly, in contrast to the lines pointing inwards, due to ($\bar{1}$ 1 1) and (1 1 $\bar{1}$).

For sliding at $\phi = 330°$ the pattern at 4 N and 400 $\mu m\,sec^{-1}$ is less wide with long lines in the centre (Fig. 4a). The (0 1 0) and (1 0 0) lines point inwards and show a regular pattern. The lines transverse to the groove are due to (1 1 $\bar{1}$) and (1 1 $\bar{1}$). As before, these are connected to the {1 0 0} lines (Fig. 4b).

The profiles of the grooves are different as well, for $\phi = 30°$ the groove has a flat bottom with small dikes

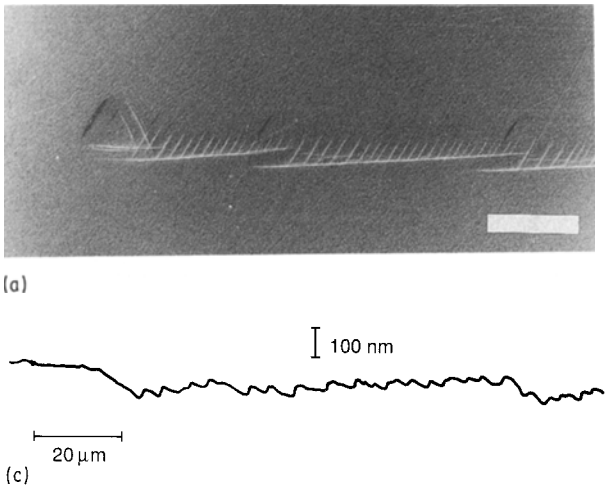

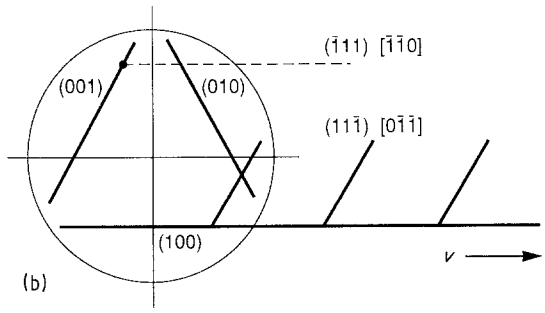

Figure 2 Groove made along [0 1̄ 1] at a load of 4 N and a speed of 400 μm sec^{-1}. (a) The start of a single pass. (b) Interpretation of the lines. Schematic drawing of the lines on the surface when (1 0 0) slip is activated (the base line) and repeated crossings occur to {1 1 1}. From the (0 0 1) side of the triangle in some cases the (interrupted) line due to cross-slip to (1̄ 1 1)[1̄ 1̄ 0] is seen. (c) Profile of the lower part of the groove in (a).

on the sides (Fig. 3c), whereas for $\phi = 330°$ the groove is narrow with only one dike (Fig. 4c). The dikes correspond to the patterns; for $\phi = 30°$ there are lines on both sides, for 330° there is only one (the side depending on where the profile is measured).

3.3. Repeated passes in both directions

3.3.1. Patterns

The simple pattern found at $\phi = 0°$ after one pass becomes more complicated when more passes are made. This has been investigated by reversing the motion several times over part of the length of the first groove. The first reversal shows that the base line again curves upwards (Fig. 5a). As before, there is cross-slip, now due to (1 1̄ 1)[0 1̄ 1̄] from the base line, but these (black) lines are not easily visible because of the illumination used here. In comparison to the forward sliding (Fig. 2b), the trailing side of the triangle, now due to (0 1 0)[1̄ 0 1̄] (Fig. 5b), is more abundant (see the white lines in the upper half of Fig. 5a). New is the black {1 1 1} line due to (1̄ 1 1)[1̄ 0 1̄], that runs parallel to the direction of sliding. It is caused by cross-slip from (0 1 0)[1̄ 0 1̄] (Fig. 5b).

The reversed motion (Fig. 5a) was reversed again, at about 200 μm from the starting point in Fig. 2a. The turning point is shown in Fig. 5c. The third pass in the same groove gives the same base line pattern with about the same number of lines. In the upper half of the groove, white lines are visible due to (0 1 0)[1̄ 0 1̄] that have been made by the second pass. There are two black lines in the upper half, one due to slip in (0 0 1)[1̄ 1̄ 0] (as in Fig. 2a) and a horizontal line, a combination of slip in (1̄ 1 1)[1̄ 0 1̄] (as in Fig. 5a) and in (1̄ 1 1)[1̄ 1̄ 0], shown in Fig. 2b. The density of (white) lines that cross-over from the base line has not increased in comparison to Fig. 1a. The length of these lines has not changed either.

The motion was reversed several times. When six passes have been made, three in each direction, the pattern can still be recognized (Fig. 5d). It is again a combination of a forward pass (Fig. 2a) and a backward pass (Fig. 5a). There is no difference between the base lines in Figs 5c and d, nor are the density and length of the cross-over lines markedly increased. What does increase is cross-slip in the upper half of the groove, where the black lines, due to (1̄ 1 1) (with two Burgers' vectors), are more abundant.

3.3.2. Cracking

When 300 passes have been made in both directions, at the lower load of 3 N, the groove has changed its appearance. Cone cracks are present on one side of the groove, easily visible after etching (Fig. 6). Note that a single pass at 3 N does not produce a groove or a line pattern.

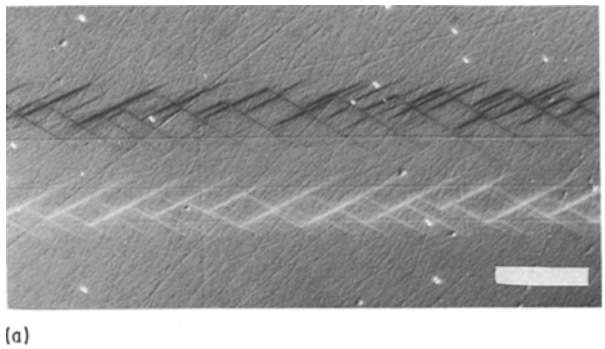

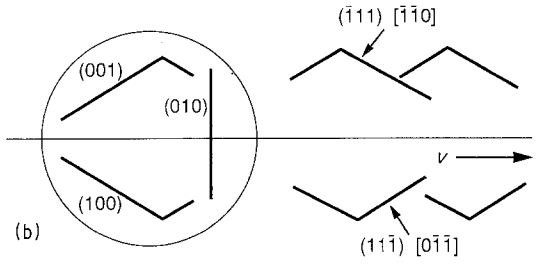

Figure 3 (a) Groove made by a single pass at 4 N and 400 μm sec^{-1} for $\phi = 30°$. (b) Interpretation of the lines in (a). Cross-slip is indicated from (0 0 1) to (1̄ 1 1) and from (1 0 0) to (1 1 1̄). (c) The transverse profile shows two dikes and a wide groove.

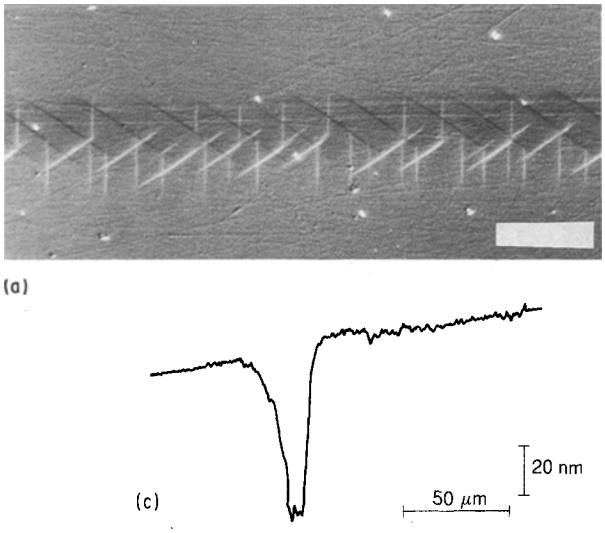

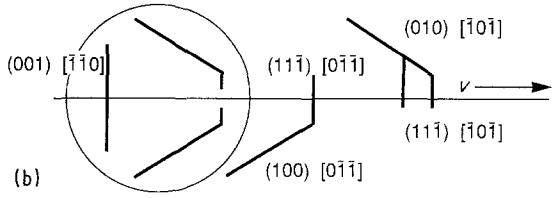

Figure 4 (a) As Fig. 3a for $\phi = 330°$. (b) Interpretation of the lines. Cross-slip now gives lines perpendicular to the groove. (c) The transverse profile shows a narrow groove without dikes.

3.3.3. Debris

When the load is lowered to 0.5 N, the number of passes can be raised considerably, without deterioration of the surface by cracking. At $N = 1000$ (in both directions, $\phi = 30°$ and 210°) a shallow groove is made with a rather smooth appearance. The dikes along the sides are flattened. Outside the groove a powder is found at a distance of about 48 μm, whereas the groove width is 28 μm (Fig. 7). At the start ($N = 1$) the width is about equal to the Hertzian diameter of the contact circle, 17 μm, so after 1000 passes the groove has widened considerably.

The origin of the powder is seen in the following experiment. At a much lower speed, $v = 4\,\mu\text{m sec}^{-1}$, and a load of 3 N, a single pass was made along $\phi = 30°$. At the start of the groove, slip lines are found, as before (Fig. 8a). Further down the groove the pattern is disturbed by wavy lines parallel to the groove (Fig. 8b). Some of the lines were already present near the start as straight lines. At the end of the groove the parallel lines are abundantly present, while the slip pattern can hardly be recognized (Fig. 8c). After one pass the groove has become nearly continuous. The slip steps have disappeared, probably by fracture. These steps are the most likely source of the fine particles that cause the parallel scratches. Some particles are moved sideways, after many more passes of the sphere, and produce the powdery debris in Fig. 7. When the sphere is inspected after three (single-pass) grooves, rings of debris are seen (Fig. 8d), at diameters of 27 and 42 μm. The groove width in this experiment is 29 μm.

4. Angular dependence

4.1. Groove depth

At $v = 400\,\mu\text{m sec}^{-1}$ single-pass grooves were made along various directions, from 330° to 30° in steps of 5°. Because at this speed a load of 3 N is insufficient to give a groove, the experiments were done at 4 N. The coefficient of friction is low, $f = 0.1 \pm 0.05$, with no significant variation with angle.

The depth of the grooves was measured at five positions, giving the average depth (in the range from 40 to 115 nm) and the standard deviation (5 to 20 nm). The depth increases by about 10 nm from 0° to 30° and by about 20 nm from 330° to 0° (Fig. 9). The difference in profile between the end points was given in Figs 3c and 4c. There is evidence of dips in the depth curve at about 340° and 25°, that are significant in view of the spread in the data.

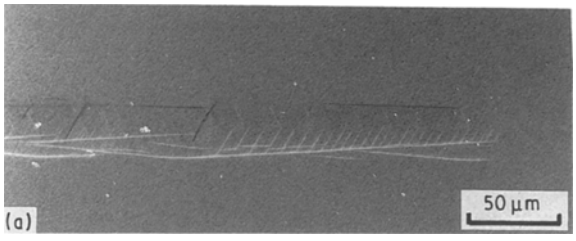

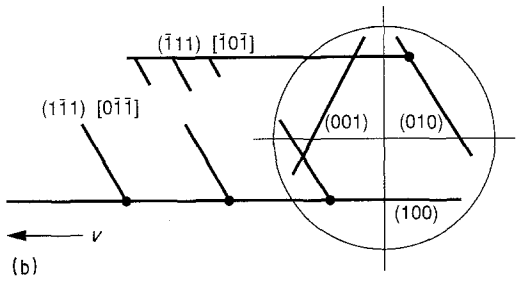

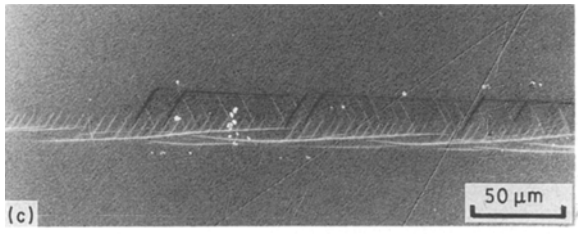

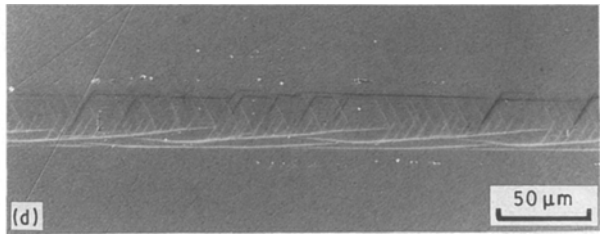

Figure 5 (a) Groove as in Fig. 2a, with one reversed pass coming from the left, to about half-way down the photograph. (b) Interpretation of the lines in (a). The horizontal line from the top of the triangle is due to $(\bar{1}\,1\,1)[\bar{1}\,0\,\bar{1}]$. (c) Groove as in (a), after one more reversal of sliding. (d) Centre of the groove, where three passes have been made in both directions.

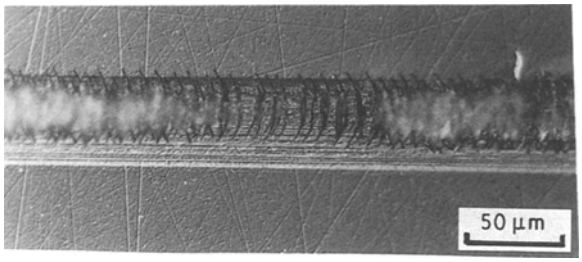

Figure 6 Groove along $\phi = 30°$ at 3 N, 400 μm sec^{-1} and 300 passes in both directions, showing cone cracks, after etching in H_2SO_4 with zinc addition.

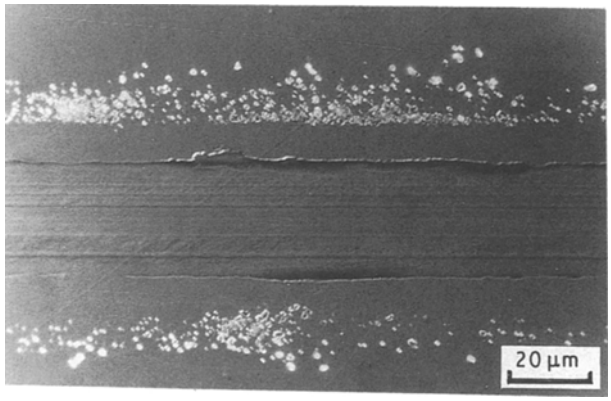

Figure 7 Groove along $\phi = 30°$ at 0.5 N, 400 μm sec^{-1} and 1000 passes in both directions. Powder-like debris is lying along the groove.

4.2. Patterns

Information on the patterns in the groove was shown for $\phi = 330°$ (Fig. 4a), 0° (Fig. 2a) and 30° (Fig. 3a). For 330° the (1 0 0) and (0 1 0) lines (cf. Fig. 4b) are slightly curved. For $\phi = 345°$ (Fig. 10) the black (0 1 0)[$\bar{1}$ 0 $\bar{1}$] lines are longer than at 330°, whereas the (1 0 0)[0 $\bar{1}$ $\bar{1}$] is practically absent. The (0 1 0) lines, here slightly curved too, show cross-slip to several (1 1 $\bar{1}$) [$\bar{1}$ 0 $\bar{1}$] lines (Fig. 10). The pattern changes gradually from 330° to 0°, in contrast to the dip in the groove depth (Fig. 9).

For $\phi = 30°$ the (1 0 0) and (0 0 1) lines (cf. Fig. 3a) are rather weak and at irregular intervals. The corresponding cross-over lines, (1 1 $\bar{1}$)[0 $\bar{1}$ $\bar{1}$] and ($\bar{1}$ 1 1) [$\bar{1}$ $\bar{1}$ 0], show a more regular pattern. This again is reminiscent of the comb patterns at $\phi = 0°$ (Fig. 2a).

The line density was obtained from the photographs. For some systems the number of lines that can be counted increases with the magnification. The data for $\times$ 727 are given in Table II. The larger groove depth at $\phi = 30°$ corresponds to a higher line density when compared to 330°. For $\phi = 0°$ there are two long, practically continuous, lines, which prevents a correlation of line density with depth.

4.3. Resolved shear stress

The calculations of the resolved shear stress (RSS) given in [11] for indenting (1 1 1) have been extended to include the effect of a friction coefficient of 0.10. In general, the effect of friction is to increase the RSS for slip planes in front of the sphere. The {1 0 0}⟨0 1 1⟩ and {1 1 1}⟨0 1 1⟩ values split up from the zero friction values of RSS/P_0 = 0.308 and RSS/P_0 = 0.247 to two or three different values, depending on the direction of sliding, i.e. the direction of the tangential load on the sphere. For the symmetrical patterns the RSS/P_0 values are given in Table II. The corresponding value of P_0 is 6.74 GPa for a load of 4 N, the radius of the contact circle is 16.8 μm.

The variation in RSS for the three {1 0 0}⟨0 1 1⟩ systems is between 2.03 and 2.13 GPa, less than 5%. The number of lines, however, varies considerably more (Table II). At $\phi = 30°$ the largest RSS/P_0 of 0.316 is calculated for slip in (0 1 0)[$\bar{1}$ 0 $\bar{1}$]. The lines are as expected perpendicular to the groove (Fig. 3b) and are observed at low speed, but not at 400 μm sec^{-1}. It is therefore of interest to consider the patterns at various speeds.

5. Speed dependence

5.1. Patterns

The slip patterns are highly dependent on speed. An example is $\phi = 330°$, where at 400 μm sec^{-1} very few lines are observed at 3 N, whereas at lower speed the pattern is well developed (Fig. 11). Another example is $\phi = 30°$, where the (0 1 0)[$\bar{1}$ 0 $\bar{1}$] pattern that was missing at 400 μm sec^{-1} (Fig. 3) is abundant at 4 μm sec^{-1} (Fig. 8).

The pattern for $\phi = 0°$ at 400 μm sec^{-1} (Fig. 2a) should be compared to those at lower speeds, made in the opposite direction, $\phi = 180°$ (Fig. 12, illuminated from the south-east). The number of all lines has increased. Moreover, the (0 1 0) lines (white) connected to the long ($\bar{1}$ 1 1) lines in the upper part of the groove,

TABLE II Number of slip lines per unit length observed at $\times$ 727, F_n = 4 N and v = 0.4 mm sec^{-1} and calculated RSS/P_0 values for a friction coefficient f = 0.10

Angle, ϕ (deg)	b = [0 $\bar{1}$ $\bar{1}$]			b = [$\bar{1}$ 0 $\bar{1}$]			b = [$\bar{1}$ $\bar{1}$ 0]		
	Plane	Lines/mm	RSS/P_0	Plane	Lines/mm	RSS/P_0	Plane	Lines/mm	RSS/P_0
0	(1 0 0)	Continuous	0.309	(0 1 0)	40	0.315	(0 0 1)	16	0.303
	(1 1 $\bar{1}$)	156	0.269	(1 1 $\bar{1}$)	0	0.256	($\bar{1}$ 1 1)	Continuous	0.260
	(1 $\bar{1}$ 1)	0	0.228	($\bar{1}$ 1 1)	0	0.236	(1 $\bar{1}$ 1)	0	0.239
30	(1 0 0)	112	0.306	(0 1 0)	0	0.316	(0 0 1)	150	0.306
	(1 1 $\bar{1}$)	73	0.267	(1 1 $\bar{1}$)	0	0.246	($\bar{1}$ 1 1)	73	0.267
	(1 $\bar{1}$ 1)	0	0.231	($\bar{1}$ 1 1)	0	0.246	(1 $\bar{1}$ 1)	0	0.231
330	(1 0 0)	78	0.313	(0 1 0)	56	0.313	(0 0 1)	0	0.302
	(1 1 $\bar{1}$)	117	0.265	(1 1 $\bar{1}$)	56	0.265	($\bar{1}$ 1 1)	0	0.249
	(1 $\bar{1}$ 1)	0	0.230	($\bar{1}$ 1 1)	0	0.230	(1 $\bar{1}$ 1)	0	0.249

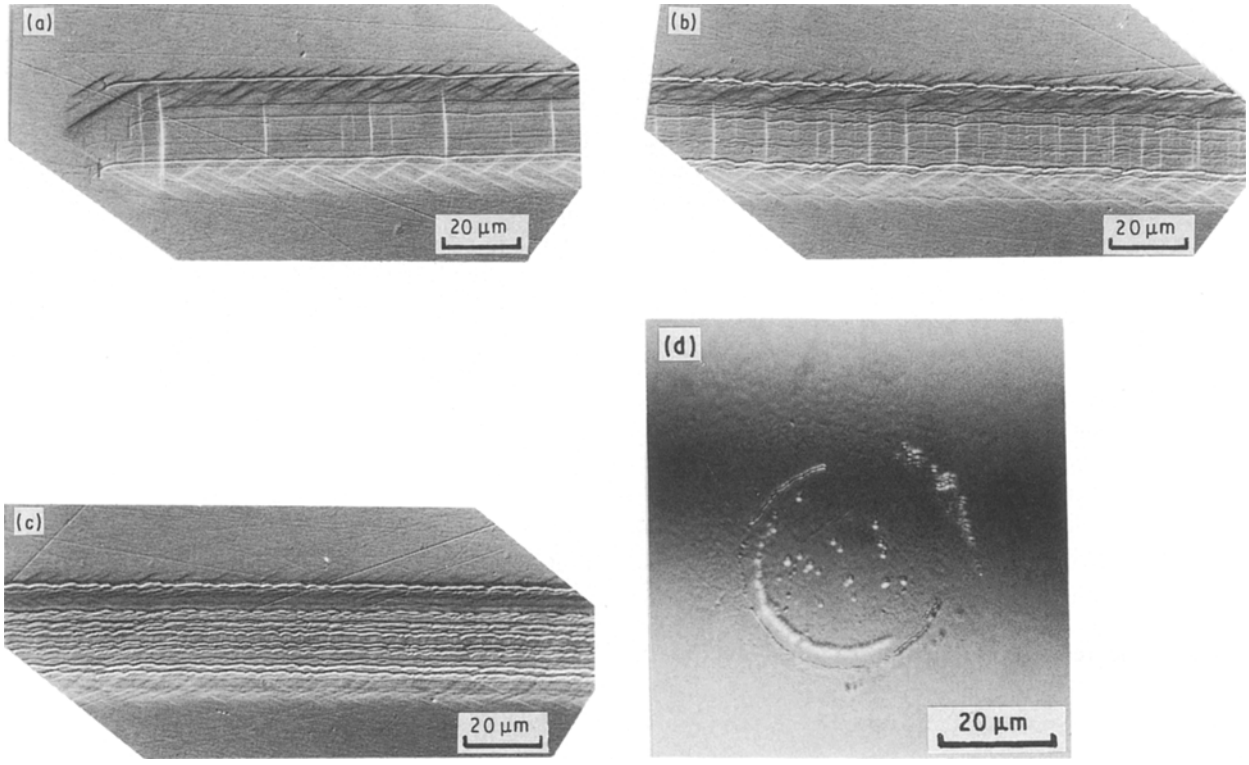

Figure 8 Groove along $\phi = 30°$ at 3 N and 4 μm sec^{-1}, showing that even for a single pass scratches occur inside the groove. (a) Start, (b), (c) further down the groove. (d) The ruby sphere shows several circles of debris after making three grooves.

are shorter, whereas the $(1\,\bar{1}\,1)$ lines (black) connected to the (1 0 0) base line still end near the centre of the groove.

5.2. Line density

The basis of the triangle is continuous when sliding along $\phi = 0°$. The other $\{1\,0\,0\}$ lines, however, decrease considerably in number at higher speed (Fig. 12). For the other ϕ values this applies to all $\{1\,0\,0\}$ lines (Fig. 13), as far as observed – (0 0 1) is missing for $\phi = 30°$ (Fig. 4b).

At $\phi = 0°$ the $(\bar{1}\,1\,1)$ lines are parallel to the groove. These lines are very long in comparison to the lines made behind the sphere, from which they may be formed by cross-slip (i.e. (0 1 0) in Fig. 5b). The other $\{1\,1\,1\}$ lines are found to be much more dependent on speed than the $\{1\,0\,0\}$ lines from which crossing occurs. No cross-slip has been found from the lines made in front of the sphere (i.e. (0 0 1) at $\phi = 0°$ in Fig. 5b and (0 1 0) at $\phi = 30°$ in Fig. 3b).

For the three orientations the line density (measured at $\times 727$) is summarized in Fig. 13. The conclusion is that the line density depends generally more on speed for $\{1\,1\,1\}$ than for $\{1\,0\,0\}$.

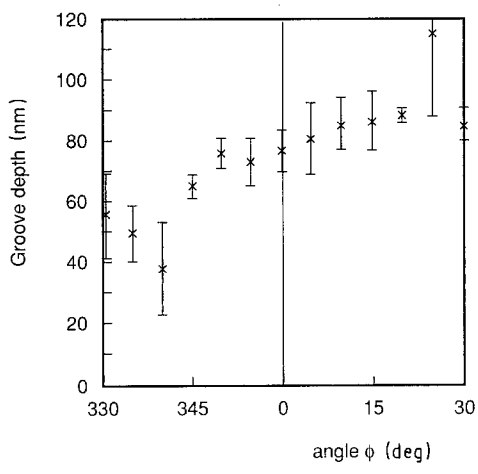

Figure 9 Depth of groove after a single pass at 4 N and 400 μm sec^{-1} for steps in ϕ of 5°.

6. Discussion

6.1. Pattern identification

In indentations, the line patterns are due to the $\{1\,0\,0\}$, $\{1\,1\,1\}$ and $\{1\,1\,0\}$ systems, where the latter was found only at higher loads as a short line. In the present work the loads are just above the threshold for slip to appear and only the $\{1\,0\,0\}$ and $\{1\,1\,1\}$ systems have been observed. Again the primary system is the $\{1\,0\,0\}$, but frequent crossings to $\{1\,1\,1\}$ have been found, for example in sliding along $\langle 0\,\bar{1}\,1\rangle$ at $\phi = 0°$, where the baseline is nearly continuous with a periodic pattern of $\{1\,1\,1\}$ connected to it. The details of the pattern will be related to the RSS below (Section 6.2). The base line is at an angle to the groove direction, it is

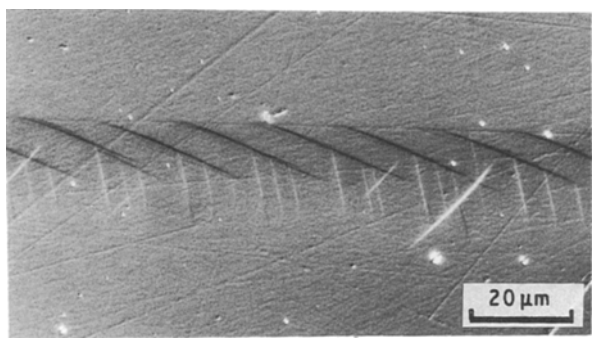

Figure 10 Grooves made at 4 N and 400 μm sec^{-1} for $\phi = 345°$.

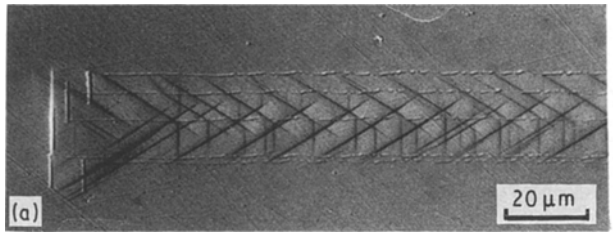

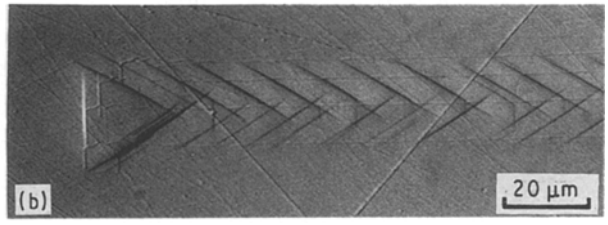

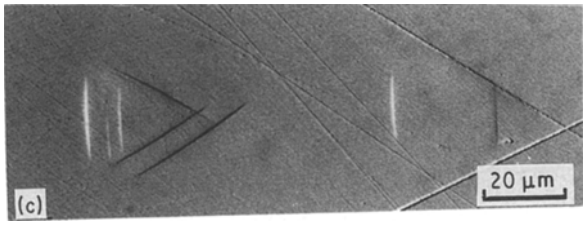

Figure 11 Grooves made at 3 N along $\phi = 330°$ for (a) 4, (b) 40 and (c) 400 μm sec^{-1}.

long but not strictly continuous and restarts are observed. A possible mechanism for the inclusion will be given in Section 6.6.

From the results of grooves made on an (1 1 0) crystal, a relation was derived between the groove depth and the resolved shear stress, where both vary considerably with the angle of sliding [11]. On the (1 1 1) crystal plane, however, the RSS for slip on {1 0 0} hardly varies with angle (Table II), hence there must be other reasons for the variation in depth.

In the groove the patterns often differ from those in indentations (Fig. 1b). There are fewer lines, especially at higher speed, and the length differs too, depending on the groove direction. The reason may be found in limitations of nucleation (Sections 6.3, 6.4) and propagation (Section 6.5).

It is interesting to note the difference in depth and number of lines between $\phi = 30°$ and 330°. In view of the symmetry of the plane these directions correspond to reversed motion. On planes with a lower symmetry the effect of motion reversal is expected to be even stronger.

6.2. The comb structure

6.2.1. The comb pattern of the base line

Several periodic patterns have been observed (Figs. 2, 3, 4, 11, 12). For sliding at $\phi = 0°$ and 180° there are two "comb-like" patterns that will be analysed in detail, one along the base line and the other from the top of the triangle (Figs 2a, 5, 12). The base line is due to slip in (1 0 0)[0 $\bar{1}$ $\bar{1}$] and cross-slip occurs to (1 1 $\bar{1}$) at regular distances (Fig. 2b). The base line is seen to be curved, the cross-slip lines become shorter and the pattern stops after 16 to 20 lines, where a new base line is starting (Fig. 2a). The top of the cross-slip lines is on a straight line parallel to the groove. The "teeth" decrease in length from 16 to 8 μm, corresponding to a shift of the base line across the groove of 0.44 μm per cross-over. The period of the teeth is 5.0 to 6.4 μm. These values should be related to the calculated radius of the contact circle, here $a = 16.8$ μm.

The following processes take place when the stress field moves with the sphere. Consider the case of Fig. 12, where the sphere moves to the left. First, as in indentations [10], slip starts in (1 0 0)[0 $\bar{1}$ $\bar{1}$], at the subsurface position (at $z/a = -0.47$, S in Fig. 14) where RSS/P_0 reaches its maximum, 0.308 (Table I). From here slip propagates in a field of decreasing RSS. At the position (C_1) where the RSS equals that for slip in (1 $\bar{1}$ 1)[0 $\bar{1}$ $\bar{1}$], cross-over to this system takes place after a distance of $0.54a$. The corresponding RSS/P_0 value, 0.247, is nearly equal to the maximum RSS/P_0 in (1 $\bar{1}$ 1)[0 $\bar{1}$ $\bar{1}$]. It is reached near the 80% contour line for (1 0 0)[0 $\bar{1}$ $\bar{1}$] slip, at C_1, from where slip proceeds on (1 $\bar{1}$ 1) to B_1, giving the first "tooth" (Fig. 14). We assume that the presence of friction does not qualitatively change this model.

6.2.2. The second tooth

Slip may now continue to propagate on (1 0 0), on (1 $\bar{1}$ 1), or on both as in indentations. If slip continues on (1 $\bar{1}$ 1) only, a number of findings may be explained. The original system (1 0 0) may be reactivated from (1 $\bar{1}$ 1), e.g. at the position B_1', because, during the motion of the sphere, the RSS on (1 0 0) becomes sufficiently large. Slip on (1 0 0) gives a line on the surface along the original direction (and from there the loop may extend in the backward direction too (Fig. 15a)). From this line slip crosses again to (1 $\bar{1}$ 1), e.g. at C_2, and a new tooth has been added to the comb (Fig. 14).

When the sphere has moved over the period of

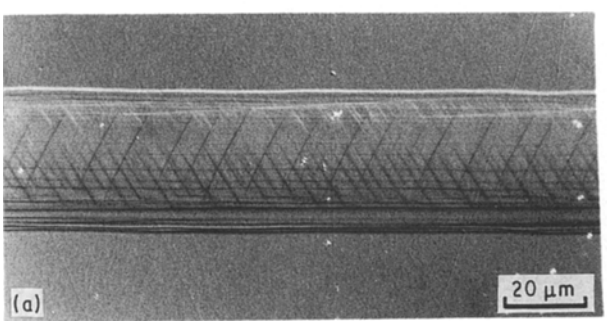

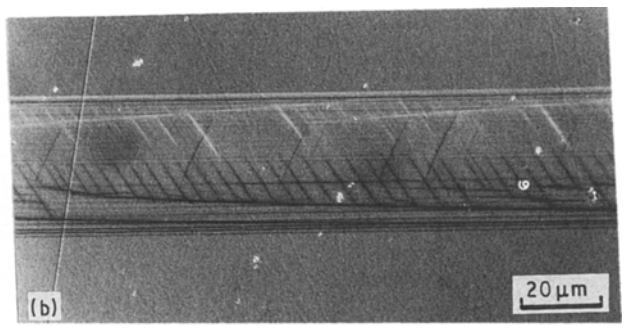

Figure 12 Grooves made at 4 N, single pass to the left and $\phi = 0°$ for (a) 4 μm sec^{-1} and (b) 40 μm sec^{-1}.

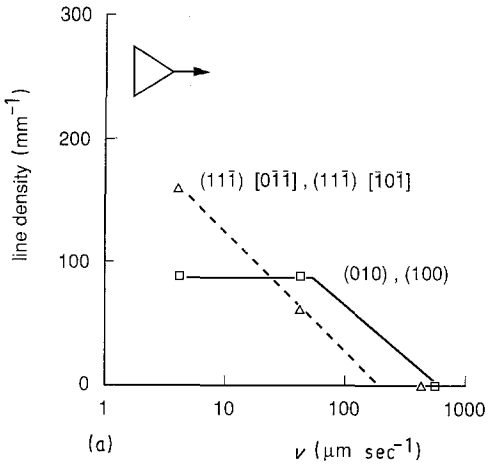

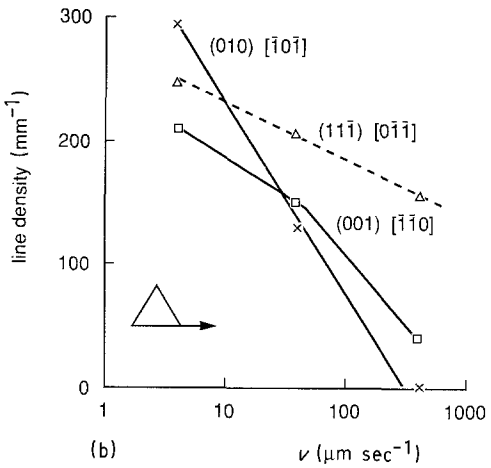

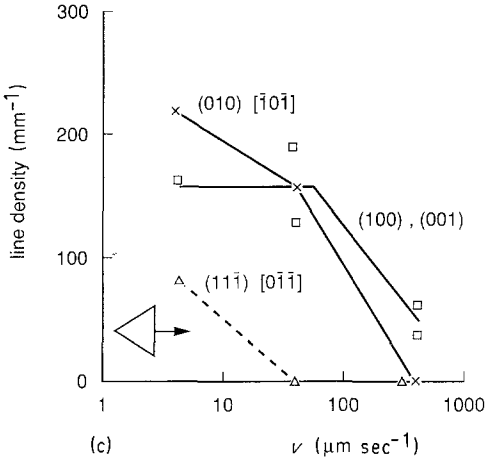

Figure 13 Line density plotted against speed of sliding for three directions. (a) $\phi = 330°$ at 3 N ($P_0 = 6.67$ GPa), (b) $\phi = 0°$ at 4 N ($P_0 = 6.74$ GPa). (0 1 0) is in front, (0 0 1) is behind the sphere. (c) $\phi = 30°$ at 3 N ($P_0 = 6.67$ GPa). (0 1 0) is in front of the sphere.

5.6 μm, i.e. $0.33a$, the RSS can be calculated to reach a value of $0.307P_0$ in (1 0 0), corresponding to 2.07 GPa, a factor 2 larger than in indentations (Table I). The observed period is therefore too large. Because approximately the same value is found for $\phi = 30°$ (Fig. 3a), it is likely that the interaction with the stress fields from the slipped {1 1 1} planes must be taken into account. The same may apply to the periodic {1 0 0} pattern for $\phi = 330°$ (Figs 4 and 11).

6.2.3. The end of the pattern

There are two reasons why the comb stops. Owing to the repeated processes, the cross-over point moves upwards and sideways, both reducing the RSS value. The sideways motion is seen in Fig. 14, where after a number of steps, the contour with RSS = $0.247P_0$ is passed at B'_3. The RSS is too low and crossing to (1 $\bar{1}$ 1) can no longer take place. The distance covered along y is then equal to SB'_3, $0.55a$, which, for $a = 16.8$ μm, is 9 μm, near the observed value. The RSS value where (1 $\bar{1}$ 1) stops can be estimated as in [10], and gives a value of 1.0 GPa, well within the range found before. Once the slip has stopped, a new activation of the original (1 0 0) system is needed and a new cycle is started.

In this argument the change of RSS in the (1 $\bar{1}$ 1) system has been neglected. Moreover, the friction has been left out, again making the agreement seem fortuitous. In any case, by a number of crossings the dislocations move out of the region of high RSS, which will eventually stop the propagation of the comb.

If the reactivation of (1 0 0) is from the first (1 $\bar{1}$ 1) system, the curvature of the base line follows from the distance covered by the slip on the (1 $\bar{1}$ 1) system. The shift along the y-axis in Fig. 14, transverse to the groove, produces the new maximum at B_1 (Fig. 15a). From here the process is repeated, at C_2(1 $\bar{1}$ 1) is excited again, after a certain distance (1 0 0) starts again, now at B_2, etc. The sequence of points, S, C_1, C_2, etc., gives a line that is inclined to the direction of sliding. If the shift per step is small, the line looks curved.

6.3. Nucleation of first slip

The variation in the number of lines on the surface, given for 400 μm sec^{-1} in Table II, and the differences in speed dependence (Fig. 13) may have several causes, differences in nucleation of slip on the {1 0 0} and {1 1 1} systems, or difficulties in propagation. Nucleation of the primary slip system will be discussed first. Owing to the small friction coefficient, there are differ-

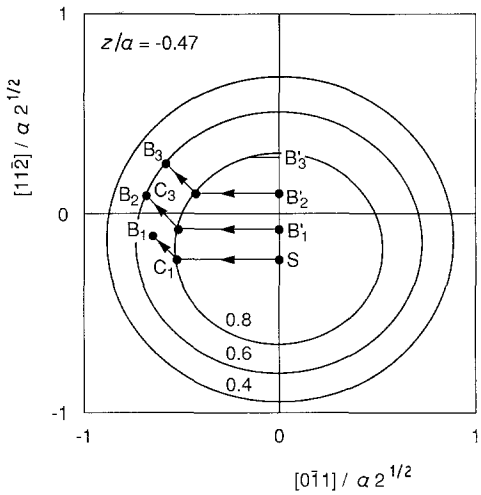

Figure 14 Contours of RSS in the x–y plane through the point of maximum RSS (S) at $z/a = -0.47$. The contours are in steps of 20% from the maximum of $0.308P_0$. C_1, C_2 and C_3 are the positions where {1 0 0} crosses to {1 1 1}. After the sphere has moved to B_1, this point is now at the centre line at B'_1, where {1 1 1} crosses back to {1 0 0}. When the 80% contour has been reached, cross-slip is no longer possible.

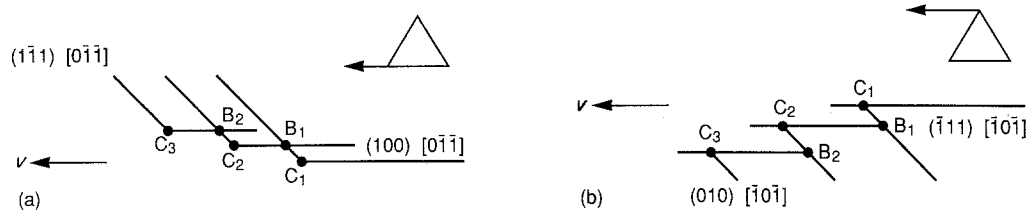

Figure 15 Interpretation of the comb pattern, observed in Figs 5a and 12. Bs and Cs as in Fig. 14. (a) Comb structure on the base line after sliding along $\phi = 0°$. (b) As (a) for the top line. At the Cs {1 1 1} crosses to {1 0 0}, at Bs {1 1 1} is activated again.

ences in the resolved shear stress (RSS) between the slip systems (Table II). The differences are small, but may be enough to favour slip on the system that can be activated in front of the sphere. Examples are the (0 1 0) slip for $\phi = 30°$, at RSS/P_0 = 0.316 (Fig. 8, the perpendicular white lines) and the same system for $\phi = 180°$ (Fig. 12a, the black lines under 60°). An example of a low RSS/P_0 value, 0.302, is for $\phi = 330°$ the (0 0 1) line, expected as a perpendicular line behind the contact, but not observed (Figs 4 and 11). For $\phi = 180°$ the (0 1 0) system has a low RSS/P_0, 0.303, but is abundantly present because it starts by cross-slip from ($\bar{1}$ 1 1), the continuous top line (Figs 5 and 12, the corresponding ($\bar{1}$ 1 1) line is not observed in Fig. 2a).

Renewed nucleation of slip seems also to be the reason for the larger number of lines, after a repeat of the sliding. The number of lines increases, but not the length (Figs 5c and d).

At higher speeds the number of lines decreases (Fig. 13), even for the lines with a high RSS/P_0, (0 1 0) for $\phi = 0°$ and 30°. By closer inspection of the lines, however, it is found that, in contrast to the number, the length of the lines does not decrease with increasing speed (e.g. Figs 12a and b). The conclusion is that propagation is not limited by lack of time, but that nucleation of slip is the rate-determining factor.

6.4. Nucleation of secondary slip

For the {1 1 1} slip systems that start by crossing from {1 0 0} there is also evidence that nucleation is necessary and that it is time dependent. From the base line in the $\phi = 0°$ triangle there is abundant crossover to (1 1 $\bar{1}$) (in Fig. 2, (1 $\bar{1}$ 1) in Figs 5 and 12), forming a comb-like structure. The length of the (1 1 $\bar{1}$) lines does not depend on speed, whereas the number of lines does (Fig. 13b).

Another example is the (even stronger) decrease in the number of (0 1 0) lines that start by cross-over from the ($\bar{1}$ 1 1) top line of the same triangle (Figs 5, 12 and 13b).

There are {1 1 1} systems with a high RSS that are absent above a certain speed, e.g. (1 1 $\bar{1}$) for $\phi = 330°$ (RSS/P_0 = 0.265) and the same system for $\phi = 30°$ with 0.267 (Figs 13a and c). The first system shows that the length of the lines decreases at higher speed (Figs 11a and b), indicating that propagation is a problem. In other examples the absence may be caused by a low RSS, the (1 1 $\bar{1}$) lines that cross-over from (0 1 0) for $\phi = 0°$ (Fig. 1b, missing in Fig. 2 at 60°, RSS/P_0 = 0.256) and for $\phi = 30°$ (Fig. 8, the cross-over at RSS/P_0 = 0.246 from the perpendicular (0 1 0) line which is missing).

6.5. Propagation limits

6.5.1. Obstructed propagation

There are also cases where the presence of other slip systems seems to hinder the propagation. For $\phi = 180°$ the trailing side of the triangle is an example (Figs 5b and 12). There are many short faint (0 0 1) lines at the edge (Fig. 12), their length decreasing with decreasing speed. The position of the lines suggests that the source is not the maximum RSS for the {1 0 0} system, which is near the centre (Fig. 1b). Instead these lines are formed near the top of the groove by cross-over from the long line on the ($\bar{1}$ 1 1) system. From here the lines propagate towards the back of the sphere (Fig. 15b). As for the base line in the same pattern, a single nucleation is sufficient for the ($\bar{1}$ 1 1) line, which explains the abundance of lines here. The shorter length of (0 0 1) at low speed may be due to the abundant presence of other lines, that hinder the nucleation of (0 0 1) or its propagation.

6.5.2. Enhanced propagation

There is a pronounced difference in the number of {1 0 0} lines between the grooves for $\phi = 30°$ and 330°, at all speeds the former exceeding the latter (Figs 13a and c). The same difference is seen in the groove depth (Fig. 9), in spite of the lower RSS/P_0 for $\phi = 30°$ (Table II). The RSS field moving with the sphere provides an explanation, because the components of slip in the direction of the motion are enhanced. This applies to $\phi = 0°$ for the long base and top lines. For $\phi = 30°$ slip towards the edges is favoured, giving a groove that is wider than the indentation. The opposite is found for $\phi = 330°$, where the motion towards the centre is enhanced, giving a narrow groove.

6.6. Curved lines

The multiple slip mechanism was used in Section 6.2 to explain the periodic cross-over patterns. It can also be used in explaining the inclination of the base and top lines for $\phi = 0°$ (Figs 5 and 12). Referring again to Figs 14 and 15, the repetition of the process gives a sequence of points, S, C_1, C_2, etc. Together these give a line that is inclined to the direction of sliding. If the shift per step is small, the line looks continuous.

In this example slip crossed from {1 0 0} to {1 1 1}, propagated over some distance on {1 1 1} and crossed to {1 0 0} again (Fig. 15a). For the horizontal line, connected to the top of the same triangle (Figs 5 and 12) crossing is from {1 1 1} to {1 0 0}, then after a short distance back to {1 1 1} again (Fig. 15b). It is interesting to note that the top line's inclination increases with

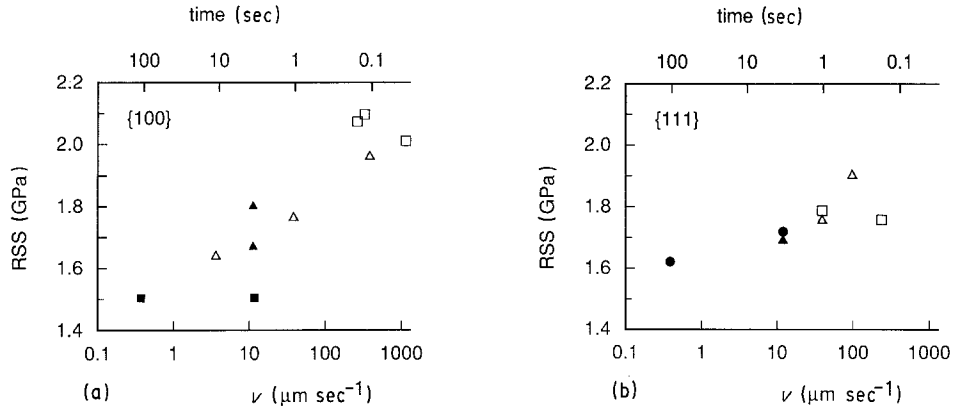

Figure 16 RSS–time diagram, showing the RSS value needed for first appearance of slip. Observations on (1 0 0) from [8], on (1 1 0) from [11] and on (1 1 1) from [10] and this paper. The solid symbols correspond to indentations, the open symbols to grooves. (a) {1 0 0} slip, observed on (△, ▲) (1 1 0) and (□, ■) (1 1 1). (b) {1 1 1} slip, on (●) (1 0 0), (△, ▲) (1 1 0) and (■) (1 1 1).

speed (Fig. 12). The angle of the base line increases with speed even more (Figs 5a and 12). The difference may be due to the time needed before cross-slip occurs. For {1 0 0} to {1 1 1} this is a faster process than the other way, as can be seen from the speed dependence of the (1 1 $\bar{1}$) and (0 0 1) lines (Fig. 13b).

A slight curvature is observed in many cases for the sides of the triangle that are well developed and extend over the width of the groove (Figs 4a, 11 and 12). The curvature may again be due to multiple slip.

The mechanism proposed here uses multiple crossings between two slip systems. This mechanism might help in explaining why a larger number of passes is more efficient than a lower speed in creating a groove. This is seen in Equations 1 to 3 for the groove depth, because C_2 is larger than C_3 [12]. The coefficients would be equal if adding another pass presents the same stress, which would double the time available for nucleation. There could be an enhancement by a second pass if it could use the {1 1 1} slip made by a previous pass, and activate {1 0 0} slip. The logarithmic dependence of depth on number of passes indicates that there is a certain saturation to the effects of another loading, i.e. the presence of a line pattern produces a certain amount of work hardening. A second reason is the decrease in P_0 when the grooves become deeper and conform more to the shape of the sliding sphere.

6.7. Speed dependence

The result of the analysis in the previous section is that nucleation is rate limiting in several cases, whereas propagation is a problem in the range of speeds used here for others (Table III). Because nucleation is possible when the resolved shear stress exceeds a certain threshold value, these values should be comparable to those from other experiments. For the two slip systems of interest, {1 0 0}⟨0 1 1⟩ and {1 1 1}⟨0 $\bar{1}$ 1⟩, the data available on the minimum RSS [9–12] have been compared with those presented here (Fig. 16). In order to compare the time of indentation with the speed of single-pass sliding, the duration of the latter was taken as $2a/v$, where $2a$ is the diameter of the contact circle. The agreement between the data is satisfactory. For {1 0 0} the RSS needed for the observation of slip, increases by about 50% when the time is decreased by three orders of magnitude (Fig. 16a). The RSS for crossing from {1 0 0} to {1 1 1} increases by about 10% over the same range (Fig. 16b).

6.8. Steps and debris

The slip steps at the surface have typically a height of 30 nm (Fig. 2c). In further contact with the sphere the steps may fracture and produce the powder that was found outside the groove (Fig. 7) or on the sphere (Fig. 8d). The sliding sphere is therefore a good example of a process where the loading produces plastic deformation, with a process-induced roughness that gives a secondary source of "abrasive" particles. By some process, here fine grooves, this finally leads the way to wear [18].

In this respect the ruby sphere has the advantage that it is hard and invariable during the experiment, with the added advantage that the stress underneath is known, as long as the elastic approximation is valid. In a number of papers, Brookes *et al.* have used low hardness sliders, where the flattening of the tip gives a constant stress, determined by the hardness [19–21]. They observed microplasticity in hard materials and studied work hardening by repeated slidings. A possible disadvantage of the use of soft sliders could be the incorporation of the wear debris into the slider, thereby limiting the length of sliding.

TABLE III Summary of the pressure (P_0) and speed of sliding (v) combinations needed for the nucleation (N) of slip. Propagation (P) was found to be limiting for some slip lines observed on (1 1 1)

Angle, ϕ (deg)	Plane	N, P	v (μm sec^{-1})	P_0 (GPa)
0	(1 0 0)	N	–	⩽2.16
	(1 1 $\bar{1}$)	N	>1000	1.81
	(0 1 0)	N	300	2.12
30	(1 0 0), (0 0 1)	N, P	(1000)	2.04
	(1 1 $\bar{1}$)	N	40	1.78
	(0 1 0)	N	300	2.11
330	(1 0 0), (0 0 1)	N	200	2.09
	(1 1 $\bar{1}$)	N, P	200	1.77

Values of v in parentheses were obtained by extrapolation in Fig. 13.

7. Conclusions

1. Grooves have been made on the (1 1 1) plane of MnZn ferrite by a sliding sphere. The depth and the slip line patterns have been studied.

2. The line patterns have been identified as belonging to the slip systems $\{1\,0\,0\}\langle 0\,1\,1\rangle$ as the primary system and $\{1\,1\,1\}\langle 0\,1\,1\rangle$ as the secondary system.

3. The excitation of the slip systems depends on the load, the speed and the direction of sliding, i.e. the direction of the friction force.

4. The angular dependence of groove depth depends on the orientation of the slip lines in the contact zone. Narrow grooves are found for $\{1\,0\,0\}$ lines growing inwards, wide grooves for lines growing outwards, the difference being due to the moving stress field. For motion along $\langle \bar{2}\,1\,1\rangle$ this effect implies that reversal of the sphere's motion gives a different groove depth.

5. Slip lines for both $\{1\,0\,0\}$ and $\{1\,1\,1\}$ increase in number at low speeds. The number of lines of the $\{1\,1\,1\}$ system has a stronger speed dependence than of the primary $\{1\,0\,0\}$ system.

6. Nucleation is rate-limiting for the majority of slip lines, both $\{1\,0\,0\}$ and $\{1\,1\,1\}$. Propagation limited by obstruction is found in a few cases only.

7. A relation was derived between the resolved shear stress for first appearance of slip and the time of loading.

8. Periodic patterns of $\{1\,1\,1\}$ lines and the curvature of $\{1\,0\,0\}$ lines have been attributed to multiple cross-slip between $\{1\,1\,1\}$ and $\{1\,0\,0\}$, by the moving stress field.

9. The slip steps lead to powder debris when the sphere moves over the steps. After more passes the debris accumulates, the sphere moves it sideways and deposits it outside the groove.

References

1. K. KUGIMIYA, E. HIROTA and Y. BANDO, *IEEE Trans. Mag.* **MAG-10** (1974) 907.
2. E. HIROTA, K. HIROTA and K. KUGIMIYA, "Recent Developments of Ferrite Heads and Their Materials", in "FERRITES", Proceedings of the International Conference, Japan, 1980, edited by H. Watanabe, S. Iida and M. Sugimoto (Centre for Academic Publications, Japan, 1981) pp. 670–4.
3. T. ITO, *J. Amer. Ceram. Soc.* **54** (1971) 24.
4. K. TANAKA, K. MIYOSHI and T. MURAYAMA, *Bull. Jpn Soc. Prec. Engng* **9**(2) (1975) 27.
5. K. MIYOSHI and D. H. BUCKLEY, *Wear* **66** (1981) 157.
6. R. P. STEIN, *ASLE Trans.* **12** (1969) 21.
7. K. F. DUFRANE and W. A. GLAESER, *Wear* **37** (1976) 21.
8. A. BROESE VAN GROENOU and S. E. KADIJK, *ibid.* **126** (1988) 91.
9. *Idem, Acta Metall* **37** (1989) 2613.
10. S. E. KADIJK and A. BROESE VAN GROENOU, *ibid.* **37** (1989) 2625.
11. A. BROESE VAN GROENOU and S. E. KADIJK, *J. Mater. Sci.* **24** (1989) 4495.
12. *Idem, Wear* **131** (1989) 353.
13. G. M. HAMILTON and L. E. GOODMAN, *J. Appl. Mech.* **33** (1966) 371.
14. G. M. HAMILTON, *Proc. Inst. Mech. Eng.* **197C** (1983) 53. The equation for σ_x due to a tangential load contains a term $x^2z^2/3$; the 3 in the denominator should be replaced by the expression S, defined in the paper.
15. G. de WITH and J. P. M. DAMEN, *J. Mater. Sci.* **16** (1981) 838.
16. S. P. TIMOSHENKO and J. N. GOODIER, "Theory of Elasticity", 3rd Edn (McGraw-Hill, New York, 1970) pp. 409 ff..
17. N. MAAN and A. BROESE VAN GROENOU, *Wear* **42** (1977) 365.
18. D. KUHLMANN-WILSDORF, "Dislocation Concepts in Friction and Wear", in "Fundamentals of Friction and Wear of Materials", edited by D. A. Rigney (American Society of Metals, Metals Park, Ohio, 1981) p. 119.
19. C. A. BROOKES, M. P. SHAW and P. E. TANNER, *Proc. Roy. Soc. (London)* **A409** (1987) 141.
20. C. A. BROOKES and A. R. PARRY, *Mater. Sci. Engng* **A105/106** (1988) 143.
21. M. P. SHAW and C. A. BROOKES, *Wear* **126** (1988) 149.

Received 13 June
and accepted 13 November 1989